Environmental Science & Technology

Article

pubs.acs.org/est

Structural Transformation of MnO_2 during the Oxidation of Bisphenol A

Sarah Balgooyen,[†] Peter J. Alaimo,[§] Christina K. Remucal,*[,†,‡] and Matthew Ginder-Vogel*[,†,‡]

[†]Environmental Chemistry and Technology Program and [‡]Department of Civil and Environmental Engineering, University of Wisconsin—Madison, Madison, Wisconsin 53706, United States

[§]Department of Chemistry, Seattle University, Seattle, Washington 98122, United States

Supporting Information

ABSTRACT: Bisphenol A (BPA) is an endocrine-disrupting compound widely used in the plastic industry and found in natural waters at concentrations considered harmful for aquatic life. BPA is susceptible to oxidation by Mn(III/IV) oxides, which are commonly found in near-surface environments. Here, we quantify BPA oxidation rates and the formation of its predominant product, 4-hydroxycumyl alcohol (HCA), in tandem with transformation of a synthetic, Mn(III)-rich δ-MnO_2. To investigate the effect of Mn oxide structural changes on BPA oxidation rate, 12 sequential additions of 80 μM BPA are performed at pH 7. During the additions, BPA oxidation rate decreases by 3 orders of magnitude, and HCA yield decreases from 40% to 3%. This is attributed to the accumulation of interlayer Mn(II/III) produced during the reaction, as observed using X-ray absorption spectroscopy, as well as additional spectroscopic and wet chemical techniques. HCA is oxidized at a rate that is 12.6 times slower than BPA and accumulates in solution. These results demonstrate that BPA degradation by environmentally relevant Mn(III/IV) oxides is inhibited by the buildup of solid-phase Mn(II/III), specifically in interlayer sites. Nevertheless, Mn oxides may limit BPA migration in near-surface environments and have potential for use in drinking and wastewater treatment.

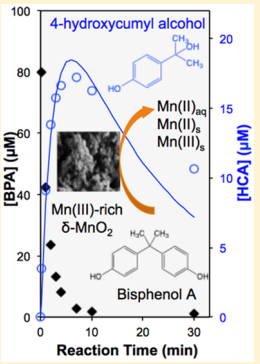

INTRODUCTION

Manganese(III/IV) oxides (MnO_x) are considered to be one of the strongest naturally occurring oxidants in near surface environments and are capable of oxidizing several classes of inorganic[1−4] and organic contaminants.[5−8] They are found in a wide range of geologic settings, including ocean floors, soils and sediments, and marine and freshwater bodies.[9−13] MnO_x oxidize many phenolic compounds, including bisphenol A (BPA).[14−16] BPA is a monomer used in the manufacture of polymeric products, such as epoxy and polycarbonate plastics.[17] It is an endocrine disruptor and, at high concentrations, has deleterious effects on the human reproductive system and child development.[18] It also leads to teratogenic, endocrine, and pleiotropic effects in aquatic species.[19] Due to its widespread use and incomplete removal during conventional wastewater treatment,[20] BPA is commonly detected in both wastewater[21,22] and surface water.[23,24]

The general transformation mechanism of phenolic compounds by manganese oxides is well-understood. Oxidation of phenolic compounds by MnO_x begins with diffusion of the organic compound to the mineral surface, followed by the formation of a surface complex.[6,7,25,26] The phenolate anion is then oxidized through a one-electron transfer via the surface complex.[6,25,27,28] The phenoxy radical formed in this process either diffuses away from the surface and reacts with other radicals to form polymeric products[5,6,25] or undergoes a second one-electron transfer to form a phenoxenium ion.[5,6,25,26,29] The phenoxenium ion can then diffuse away from the mineral surface and undergo hydrolysis to form a benzoquinone.[5,27] Up to 64% of BPA oxidized by MnO_x reacts to form 4-hydroxycumyl alcohol (HCA; Figure S1) through radical coupling.[15,30]

Mn(IV) undergoes reduction to Mn(III) and Mn(II) during its reaction with phenolic compounds, leading to changes in the overall reactivity of the oxide. The role of Mn(III) in organic compound oxidation is unclear. Mn(III) may act as a potent oxidant of organic compounds because it has a faster rate of ligand exchange[31] and a higher redox potential compared to Mn(IV).[8,28] However, the presence of Mn(III) decreases MnO_x oxidizing capacity, metal sorption capacity, and photochemical activity under some conditions.[32−38] In contrast, Mn(II) does not oxidize organic compounds. Once formed, Mn(II) initially remains sorbed on the solid and later undergoes desorption once the mineral surface reaches saturation with respect to Mn(II).[6,7,39]

The study of organic chemical oxidation by manganese oxides has evolved from examining reductive dissolution of the mineral to quantifying organic contaminant transformation. Initial studies of the oxidation of organic compounds in the presence of manganese oxides quantify reductive dissolution of the solids in the presence of high initial organic compound concentrations and suggest that the rate-limiting steps of the reaction are either the formation of the surface complex or the

Received: November 22, 2016
Revised: April 24, 2017
Accepted: April 26, 2017
Published: April 26, 2017

DOI: 10.1021/acs.est.6b05904
Environ. Sci. Technol. XXXX, XXX, XXX−XXX

first electron transfer.[6,7,26,40] Later studies determine the loss rates of the organic compounds and the organic compound transformation mechanism rather than dissolution of the mineral. In general, the degradation rate of organic compounds follows pseudo-first-order kinetics during the initial phase but later deviates from this regime.[15,26,41−43] Additionally, these studies examine changes in reaction rates with varying pH,[26,41−43] in the presence of cations,[14−16,44,45] or with dissolved organic matter.[15,16,45] While there has been little effort to comprehensively connect changes in the mineral surface with organic contaminant transformation, one previous study quantifies the decrease in Mn oxidation state after reaction with high initial concentrations of phenol, aniline, and triclosan (i.e., 1 mM) at pH 5.[46] However, the experimental conditions limit the environmental relevance of the study, and the change in oxidation state is not compared with the reaction kinetics or organic product evolution.

Here, we examine how changes to the mineral, such as the production of reduced manganese and change in structure, affect the oxidation kinetics of BPA by Mn(III)-rich δ-MnO_2, a mineral similar to biogenic birnessite.[47−50] Experiments with single additions of BPA or HCA are used to characterize the aqueous-phase kinetics and probe the reactivity of the manganese oxide. Experiments with multiple, sequential additions of environmentally relevant concentrations of BPA at neutral pH are used to induce transformations in the solid phase from repeated exposure. Although this is a simplified system, the use of multiple BPA additions simulates the continuous introduction of BPA in near-surface environments or water treatment systems. By characterizing both the solution and solid phases using a suite of complementary techniques, we provide a comprehensive conceptual model of this complex redox reaction.

MATERIALS AND METHODS

Materials. Commercially available chemicals were used as received. HCA was synthesized by modifying a previous method.[51] Ultrapure water was supplied by a Milli-Q water purification system maintained at 18.2 MΩ•cm. Further details on the materials used and the HCA synthesis are provided in section S1.

Preparation and Characterization of Mn(III)-Rich δ-MnO_2. The mineral used in this study was prepared by rapidly adding a solution of 112.9 g/L $Mn(NO_3)_2{\cdot}4H_2O$ to a solution of 24 g/L NaOH and 47.4 g/L $KMnO_4$ and stirring for at least 12 hours. The resulting slurry was centrifuged and washed five times in Milli-Q water. The solids were then suspended in Milli-Q water, stored at 4 °C, and used within 10 days. The slurry concentration was determined by gravimetric analysis. The starting material was characterized by X-ray diffraction (XRD; Rigaku Rapid II, Mo Kα source; λ = 0.7093 Å), X-ray absorption near edge structure (XANES) spectroscopy, X-ray photoelectron spectroscopy (XPS), oxalate titration,[52−54] and Brunauer−Emmett−Teller (BET) surface area measurements (Quantachrome Autosorb-1, nitrogen adsorbate). XRD showed that δ-MnO_2 was the only crystalline phase. BET measurements revealed a specific surface area of 113 ± 14 m^2/g. XANES data showed that the valence state of the starting material is 3.55 valence units (v.u.), with percentages of Mn(IV), Mn(III), and Mn(II) at 62%, 31%, and 7%, respectively. These values were corroborated by XPS, which reported 65% Mn(IV), 32% Mn(III), and 3% Mn(II). Oxalate titration resulted in a valence state of 3.66 vu. Due to its low average valence state, the starting material is considered a Mn(III)-rich δ-MnO_2, rather than a pure Mn(IV) mineral. The presence of Mn(III) in the starting material is due to incomplete comproportionation of Mn(II) and Mn(VII) during synthesis and yields a mineral similar to environmental solids.

Solution Preparation. All reactions were performed in a pH 7 solution buffered with 10 mM piperazine-*N*,*N*′-bis(2-ethanesulfonic acid) (PIPES) and adjusted to an ionic strength of 20 mM using NaCl. PIPES was selected as a buffer because it does not form complexes with Mn(II) or Mn(III)[55,56] and does not sorb to the manganese oxide surface.[57] BPA (107 mM) and HCA (10 mM) stock solutions were prepared in methanol and stored at 4 °C.

Kinetics of BPA and HCA Oxidation during Single-Addition and Triple-Addition Experiments. The initial reactivity of Mn(III)-rich δ-MnO_2 was determined using single-addition batch reactions with either BPA or HCA. BPA or HCA (80 μM) was added to a 200 mL slurry of 0.33 g/L Mn(III)-rich δ-MnO_2 in the buffered solution. The reactors were stirred at room temperature for the duration of the reaction (30 min for BPA and 90 min for HCA). A pair of reaction slurry aliquots (1 mL each) were taken at predetermined time points to quantify the concentration of BPA and HCA. A single aliquot from each time point was quenched with excess ascorbic acid (40 μL of a 280 mM stock in Milli-Q stored at 4 °C) to reduce all Mn(III/IV) solids to dissolved Mn(II), while the other aliquot was filtered through a 0.2 μm polytetrafluoroethylene filter. The samples were analyzed by high-performance liquid chromatography (HPLC; section S2). Single-addition batch experiments were conducted in triplicate and the resulting data averaged. Loss rates were determined by fitting the data by assuming pseudo-first-order kinetics (section S3). Error was calculated using the standard deviation of loss rates determined at various time points. HCA was confirmed as a product in BPA reactors using HPLC retention time and UV spectroscopy (section S4; Figures S6 and S7).

HCA production rate and yield were calculated according to

$$[\mathrm{HCA}] = k_1 \cdot F_{\mathrm{HCA}} \cdot \frac{[\mathrm{BPA}]_0}{k_2 - k_1} \cdot (e^{-k_1 t} - e^{-k_2 t}) \quad (1)$$

where k_1 is the rate constant of BPA oxidation, F_{HCA} is the fraction of BPA converted to HCA, $[BPA]_0$ is the initial BPA concentration (80 μM), k_2 is the oxidation rate constant of HCA, and t is time after BPA addition. k_1 was determined by fitting the BPA loss data by assuming pseudo-first-order kinetics (section S3). F_{HCA} was calculated by least-squares minimization (section S4).

Organic sorption was determined by comparing concentrations in quenched and filtered aliquots over three sequential additions of 80 μM BPA to the same batch of MnO_2. Quenched samples contained total BPA and HCA (aqueous and sorbed), whereas filtered samples contained only aqueous BPA and HCA. Sorbed BPA or HCA was calculated by $[BPA]_{total} - [BPA]_{aqueous}$ or $[HCA]_{total} - [HCA]_{aqueous}$, respectively.

Aqueous Chemistry during 12-Addition Experiments. The 12-addition experiments were conducted to observe changes in BPA oxidation kinetics with repeated exposure. Mn(III)-rich δ-MnO_2 was reacted with BPA in duplicate 6 L batch reactors containing 0.33 g/L MnO_2 in pH 7 buffered solution. BPA (80 μM) was introduced into the reactor at each of the 12 additions. Concentrations and addition intervals were

DOI: 10.1021/acs.est.6b05904
Environ. Sci. Technol. XXXX, XXX, XXX−XXX

dictated by the number of electrons estimated to induce structural changes.[2] Reaction durations were determined by preliminary work. The first two reactions lasted 1 h, the third was 1.5 h, the fourth was 3 h, the fifth was 6 h, and reactions 6−12 were each 12 hours in duration. The volume of BPA stock added was <0.8% of the reactor volume per addition. No variation in pH was observed over the course of the experiments. Aliquots were removed at predetermined time points and quenched with excess ascorbic acid, as described above, and used to quantify total BPA and HCA concentrations using HPLC (section S2). Additionally, dissolved Mn was quantified in filtered aliquots (0.2 μm polytetrafluoroethylene filters) by inductively coupled plasma-optical emission spectroscopy (ICP-OES; section S2) at the end of each reaction period.

Characterization of the Solid Phase from the 12-Addition Experiments. Mn oxide solids obtained after each of the 12 additions of BPA were analyzed to determine mineralogical transformations. At the end of each reaction period, solids were collected by vacuum filtration (0.7 μm borosilicate glass fiber filters) of 150 mL of slurry from each duplicate reactor. The solids were then rinsed with methanol to desorb organic reaction products and quench the reaction. The solids from both reactors were dried at room temperature, combined, ground, and used for solid-phase characterization. Solids were characterized using XRD, calcium exchange, and spectroscopic analysis, as described below.

XPS was performed using a Thermo Scientific K-Alpha XPS system with an Al Kα X-ray source. Spectra from the Mn3*p* orbital were collected and analyzed to quantify the oxidation state of the multivalent manganese oxides. Briefly, data was processed in CasaXPS (2016 Casa Software Ltd.) using Shirley background subtraction and fit using a packet of correlated component peaks representing each possible oxidation state.[58] The binding energies, intensities, and peak widths were allowed to vary. At these energies, XPS is expected to interrogate only the top 10−50 Å of aggregated particles (not crystalline domains); therefore, results are reported as a percentage of surface Mn(IV), Mn(III), and Mn(II).

Extended X-ray absorption fine structure (EXAFS) and XANES data were collected at beamline 13-BM-D at the Advanced Photon Source at Argonne National Laboratory. This beamline has a bending magnet source equipped with a Si(111) double crystal monochromator, which was detuned by 40%. Samples were prepared by diluting 18 mg of solid MnO_2 in 72 mg of boron nitride and ground until homogeneous. Data was collected at room temperature in both transmission and fluorescence (Canberra 16-element Ge detector). Successive XANES scans were identical, indicating no change in Mn oxidation state during data collection. XANES and EXAFS data were processed using SIXPack.[59] XANES data were fit using the multistandard Combo method[60] by fitting the first derivative of the XANES spectra with restriction to a non-negative fit. XANES and EXAFS spectroscopies interrogate the average environment of all Mn nuclei in the sample and are therefore reported as the bulk valence state and percentages of bulk Mn(II), Mn(III), and Mn(IV). EXAFS fitting was done using a full, multiple scattering model of layered Mn oxides.[2,61] Phase and amplitude files were created using FEFF 7.2.[62] SIXPack's FEFF EXAFS fitting uses IFEFFIT as its primary fitting algorithm, and fits were optimized by minimizing X^2.[63] The EXAFS model accounts for splitting of Mn−O and Mn−Mn distances in the MnO_6 octahedral layer due to Jahn−Teller distortion, out-of-plane bending of the octahedral layer, vacancies in the Mn octahedral layer, and interlayer cations. Production of reduced manganese within the layer is detected by a change in the fractional occupancy of manganese centers within the layer as they fill in the vacancies in a Mn(IV) phyllomanganate structure.[35,48,64] Reduced manganese sorbed onto the layer is detected by Mn at a slightly longer interatomic distance than the other Mn centers. This is because sorbed Mn generally forms a corner-sharing complex with an interatomic distance of 3.45 Å, while Mn centers within the layer have an interatomic distance of 2.85−2.95 Å.[61]

Calcium exchange experiments were performed to quantify Mn(II) sorbed on the surface of the solid phase. Weighed samples were suspended in 10 mM PIPES (pH 7) with 25 mM $CaCl_2$ and placed on a shaker table for 48 h. After 48 h, aqueous Mn(II) that was displaced by Ca^{2+} was quantified by ICP-OES.

RESULTS

Kinetics of BPA and HCA Oxidation during Single-Addition and Triple-Addition Experiments. When BPA is exposed to Mn(III)-rich δ-MnO_2, rapid oxidation of BPA occurs (Figure S8). The loss of BPA initially follows pseudo-first-order kinetics, with a loss rate of 0.585 min^{-1} over the first 4 min of the reaction. However, the reaction rate of BPA oxidation deviates from pseudo-first-order kinetics if the first 10 min of the reaction are considered (Figure S4). HCA appears in solution immediately after BPA addition; however, it is also oxidized by MnO_2 and does not accumulate in solution during single-addition experiments (Figure S8). The molar yield (mol HCA produced/mol BPA consumed) of HCA production from BPA oxidation is 32% for the 30 min reaction.

Additional experiments are conducted with HCA as the target organic compound to quantify its oxidation rate due to reaction with Mn(III)-rich δ-MnO_2. The oxidation rate of HCA by MnO_2 is 0.0465 min^{-1} over the first 10 min of reaction, which is 12.6 times slower than that of BPA under the same conditions (Figures S4 and S5). The slower oxidation of HCA by MnO_2 relative to BPA is similar to a previous report, which found HCA to react 5 times slower.[30] As observed for BPA, the loss rate of HCA deviates from pseudo-first-order kinetics over longer reaction periods (e.g., 60 min; Figure S5).

The amount of sorbed BPA and HCA is determined by quenching the reaction using two different methods (i.e., ascorbic acid addition or filtration). Over three additions of BPA to a batch of MnO_2, BPA sorbs to the surface during the first addition (14.3 ± 7.4% of total BPA) but not during the second and third additions (Table S2). The amount of HCA generated as a product of BPA oxidation and then subsequently sorbed on the surface is negligible during the first addition but increases with each addition of BPA up to 1.0 ± 0.9% in the third addition.

Aqueous Chemistry during 12-Addition Experiments. A total of 12 sequential additions of BPA are used to induce structural changes and to probe how the reactivity of the Mn oxide changes during the reaction. This approach allows the observation of the effects of repeated exposure of an environmentally relevant amount of BPA to Mn(III)-rich δ-MnO_2.

Over sequential additions of BPA to the same batch of MnO_2, both the BPA oxidation rate and the yield of HCA decrease with each addition. The first-order rate constant after one addition of BPA is 0.56 min^{-1} ($t_{1/2}$ = 1.24 min), while the

DOI: 10.1021/acs.est.6b05904
Environ. Sci. Technol. XXXX, XXX, XXX−XXX

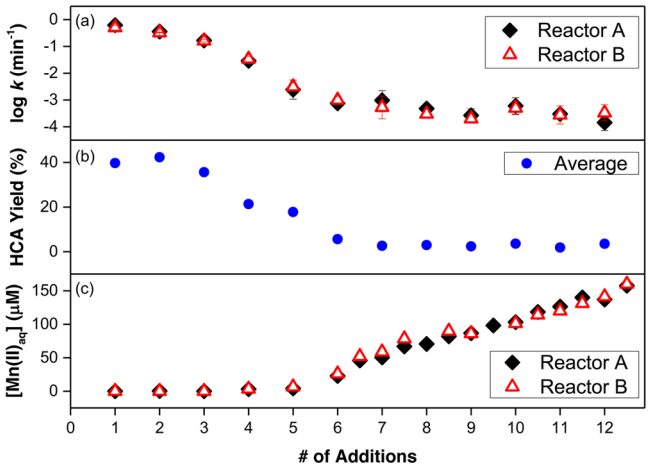

Figure 1. (a) BPA pseudo-first-order loss rate constants for duplicate reactors, (b) HCA production yield as a percent of oxidized BPA for reactor averages, and (c) aqueous manganese concentrations for duplicate reactors over 12 additions of 80 μM BPA with 0.33 g/L of Mn(III)-rich δ-MnO_2 in a PIPES buffer (pH 7). Error bars for aqueous manganese concentrations are smaller than data point size.

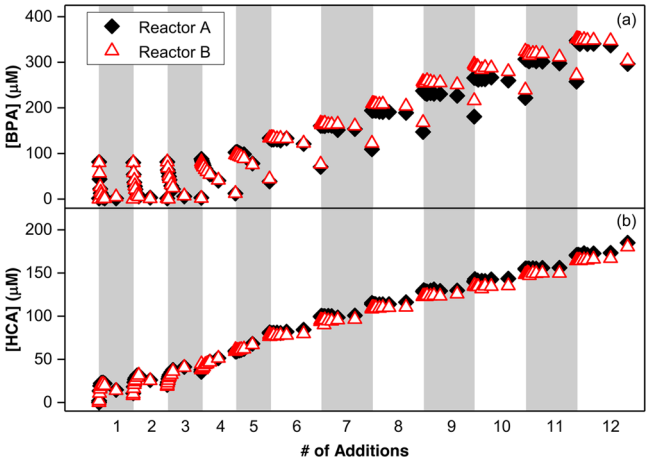

Figure 2. (a) BPA and (b) HCA concentrations over 12 additions of 80 μM BPA with 0.33 g/L of Mn(III)-rich δ-MnO_2 in a PIPES buffer (pH 7). Data sets are for duplicate 6 L reactors. Note that kinetic data is collected in the first hour of each addition, but the total lengths of additions are not the same. The first two additions were 1 h, the third was 1.5 h, the fourth was 3 h, the fifth was 6 h, and additions 6–12 were 12 hours.

rate constant after 12 additions of BPA is 2.38×10^{-4} min^{-1} ($t_{1/2}$ = 2910 min; Figure 1a). After the fifth addition, BPA is not completely consumed within the allotted reaction time and begins to accumulate in the reactors (Figure 2a). The main oxidation product, HCA, appears immediately in the reactors but is quickly oxidized by the Mn(III)-rich δ-MnO_2. After three additions of BPA, HCA begins to accumulate in solution (Figure 2b). Assuming that the ratio between BPA and HCA loss rates remains constant (i.e., 12.6:1), the mole percent of BPA converted to HCA decreases over the sequential-addition experiment. After the first addition of BPA, 39.7% of added BPA is recovered as HCA. After the 12th addition, only 3.5% of added BPA is recovered as HCA (Figure 1b; Table S1).

Aqueous manganese is not present above the detection limit after the first five reactions with BPA. After the sixth addition of BPA, aqueous manganese begins to accumulate in solution (Figure 1c). By the end of the 12th addition of BPA, 2.6% of the total Mn (158.7 μM) is in solution. Strong ligands (e.g., pyrophosphate, citrate, or ethylenediaminetetraacetic acid) are required to solubilize Mn(III).[65] Therefore, it is likely that the aqueous manganese detected is predominantly Mn(II).

Solid-Phase Changes during 12-Addition Experiments. The valence state at the surface of the mineral is measured using XPS, which probes only the top 10–50 Å of the aggregated particles at this energy. These aggregates are estimated to be hundreds of nanometers in diameter.[50] A sample of the fitted data is provided in Figure S11. Overall, the amount of surficial Mn(III) increases while Mn(IV) decreases during sequential additions of BPA (Figure 3a). For example, surface Mn(III) increases from 32% (initial material) to 42% after the sixth addition, then decreases to 37% by the end of the 12th addition. Conversely, surface Mn(IV) decreases from 65% (initial material) to 56% after the sixth addition, then increases slightly to 60% after the 12th addition. A low percentage of solid Mn(II) is detected by XPS (3–10%), with no observable trends.

The speciation and average oxidation state of the bulk solid is measured by XANES spectroscopy, which probes the entire sample. An example of the fitted data is provided in Figure S12. Over 12 additions of BPA, bulk Mn(III) decreases from 31% to 25%. As bulk Mn(III) decreases, the quantity of bulk Mn(IV) increases from 62% to 69% (Figure 3a). A small amount of solid Mn(II) is detected in all samples (i.e., 3–5% in all analyzed samples), with no observable trends. The quantification limit for Mn(II) in this technique is 5% by mole Mn.[60] The bulk valence state for the starting material (3.55 v.u.) increases to 3.63 v.u. by the end of the 12th addition (Figure S13). The accuracy of this method is 0.04 v.u.[60]

Analysis of the EXAFS data (Figure S14) using a full, multiple scattering model reveals that the fractional occupancy of Mn within the layer increases slightly upon reaction with BPA (Table S4) but does not follow a notable trend throughout the experiment (Figure 3b). Solids from the first three additions of BPA have no detectable corner-sharing Mn centers. After the fourth reaction with BPA, corner-sharing Mn centers are detected, and its coordination number steadily increases until the end of the experiment (Figure 3b).

Changes in surface area over the 12 additions of BPA were negligible, as observed by BET measurements (Table S3). XRD data (Figure S15) show that no new phases form over 12 additions of BPA. However, qualitative changes in the diffraction pattern are observed, such as the reduced tailing of the *hkl* diffraction band at 37° and the appearance of a dip at ~47° after 12 additions of BPA.

Calcium exchange experiments show that Ca^{2+}-extractable Mn(II) increases with increasing additions of BPA (Figure S16). After the first addition of BPA, 0.11 μg/mg is extracted from the solid, while after seven additions of BPA, 2.88 μg/mg is extracted. The amount of Ca^{2+}-extractable Mn(II) remains constant for the remainder of the experiment. Control experiments using only PIPES pH 7 buffer show that very little Mn is extracted in the absence of Ca^{2+} (i.e., 0–0.4 μg/mg).

DISCUSSION

Deviation from Pseudo-First-Order Kinetics. The oxidation rate of model compounds[6,7,25,41,66–68] and BPA[14,15] follow pseudo-first-order kinetics during the initial phase of the reaction, but the rates of oxidation decrease as the reaction

DOI: 10.1021/acs.est.6b05904
Environ. Sci. Technol. XXXX, XXX, XXX–XXX

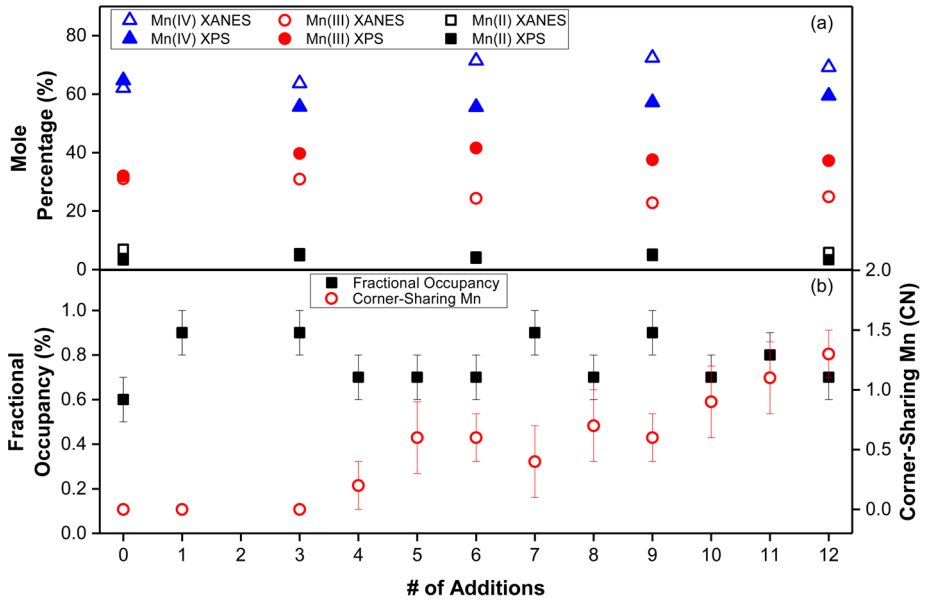

Figure 3. (a) Mole percentages of Mn(II), Mn(III), and Mn(IV) in a subset of solid samples determined by both XPS and XANES, and (b) variables obtained from the EXAFS spectra modeling of solids obtained over 12 additions of 80 μM BPA with 0.33 g/L of Mn(III)-rich δ-MnO_2 in a PIPES pH 7 buffer. Corner-sharing Mn is reported as coordination number (CN). Error for fractional occupancy and corner-sharing Mn was calculated by SIXPack during the modeling process. Samples from both reactors were combined and then analyzed.

proceeds. Previous studies show that the oxidation rates deviate from pseudo-first-order kinetics but generally only examine solution kinetics during the first phase of the reaction by using the initial rate approach.[14,15,41−46] A limited number of studies examine longer reactions by fitting data using empirical or semiempirical equations[42,69] or by applying a kinetic model based on the observed organic compound loss rate and the number of reaction sites.[40] Here, this same kinetic deviation is observed in single addition batch experiments of BPA (Figure S4). Furthermore, the decrease in reactivity of the Mn oxide due to reaction with the phenolic contaminant is clearly observed in experiments with 12 sequential additions of BPA, with BPA oxidation rates slowing by 3 orders of magnitude over the course of the reaction (Figure 1a).

The connection between changes in oxidation kinetics and the mineral surface has not been closely examined. Previous studies demonstrate that the addition of aqueous Mn(II), which is a product of the reductive dissolution of MnO_x, inhibits organic contaminant oxidation rates.[14,15,44,45] This indicates that the accumulation of Mn(II) can change the reactivity of the mineral surface but does not provide direct mechanistic evidence. Another study observes changes in MnO_x oxidation state after a single exposure to triclosan, aniline, and phenol.[46] An increase in the amount of Mn(II) and Mn(III) on the surface of the Mn oxide was detected by XPS but not linked to the target organic oxidation kinetics. In the present study, changes in oxidation kinetics and concurrent structural changes are explored using a wide range of analytical techniques to examine both solution and solid-phase chemistry. The results are used to systematically evaluate potential factors that may lead to the widely observed decrease in manganese oxide reactivity after exposure to organic target compounds.

Changes in Surface Area. Because the reaction between Mn oxides and target organic compounds occurs on the surface of the mineral,[41] changes in MnO_x surface area can potentially affect the reactivity of MnO_x by decreasing the number of available reactive surface sites.[70] However, only minor changes in the surface area are observed over the course of 12 additions of BPA (Table S3). The lack of correlation between changes in surface area and the wide range of BPA oxidation rates observed in this study (Figure 1a) indicates that the decrease in oxidation rate cannot be attributed solely to a decrease in overall number of reactive sites; however, this measurement does not account for changes in interlamellar spaces and micropores.

Changes in MnO_x Average Oxidation State. A decrease in average oxidation state could affect the reactivity of the solid by decreasing the rate of electron transfer.[40] Changes in average oxidation state have been reported under some conditions. For example, the oxidation state of a synthetic Mn(III/IV) oxide, determined with XPS, decreases from 3.7 to 3.3 v.u. after reaction with 1 mM triclosan for 24 h at pH 5.[46] In this study, repeated reaction of MnO_2 with 80 μM BPA for variable experimental durations (i.e., 1−12 h for 12 sequential additions) at pH 7 decreases the surface oxidation state by 0.09 v.u. (quantified by XPS) and increases the bulk oxidation state by 0.08 v.u. (quantified using XANES; Figure S13). At this energy, XPS only probes the top 10−50 Å of the aggregated particles. The increase in bulk oxidation state throughout the reaction is likely due to the dissolution of Mn(II) during manganese reduction, lowering the fraction of reduced Mn centers present in the solid. The valence state at the mineral surface, as determined by XPS, differs from the bulk, decreasing slightly over the 12 additions of BPA (Figure S13). This small change may be one explanation for the decrease in oxidation rate, and the increasing disparity between the bulk and surface oxidation state may imply that electrons are not being conducted throughout the mineral assemblage and accumulate at the surface.

Differences in the change in average oxidation state between this study and prior reports of a large decrease in average oxidation state[46] may be attributable to the differences in the experimental conditions. While both studies use Mn(III)-rich δ-MnO_2 synthesized with similar methods and examine the

DOI: 10.1021/acs.est.6b05904
Environ. Sci. Technol. XXXX, XXX, XXX−XXX

oxidation of phenols, major differences between the studies remain. First, while the initial organic compound concentrations in the two studies are quite different (i.e., 80 μM compared to 1 mM), the total amount of BPA added in this study over the course of 12 additions is similar (i.e., 0.96 mM). Second, the total experimental duration in this study is 96.5 h, compared to 24 h. Finally, the oxidation of organic compounds by Mn oxides is highly pH-dependent and typically faster under acidic conditions;[26,41−43] although the initial rates of organic compound oxidation were not reported in the previous study, less than 30 μM of triclosan, phenol, and aniline remained in solution after only 5 min of reaction at pH 5. Additionally, the rate of Mn(III) disproportionation into Mn(II) and Mn(IV) increases in conjunction with pH,[65] which could result in additional Mn(IV) accumulation on the mineral surface with concomitant Mn(II) production and release into solution. Collectively, these differences suggest that a rapid reaction with a high initial organic concentration is needed to induce substantial changes in Mn oxidation state, whereas a more gradual reaction of the same total amount of organic results in very small changes in the Mn oxidation state.

Sorption of BPA and Organic Products. Sorption of the target organic compound (i.e., BPA) may enhance the overall reactivity of MnO_x by facilitating the formation of a surface complex, while the sorption of organic reaction products (e.g., HCA) can decrease reactivity by obscuring reactive sites on the surface.[25,26,40−42,66] Sorption of organic compounds depends on both the type of compound and the experimental conditions (e.g., pH). For example, sorption of sulfonamides,[71] lincosamides,[72] and carbamazepine[73] to Mn oxides is negligible. In contrast, sorption of triclosan to δ-MnO_2 can be extensive, primarily under acidic conditions (e.g., 55% sorbed at pH 5 and 10% sorbed at pH 8).[26] While the sorption of organic transformation products on Mn oxides has received little attention, one previous study observes increased carbon and chlorine on the mineral surface after reaction with triclosan at pH 5, indicating that there are organic species sorbed on the mineral.[46]

Here, over three additions of BPA, sorption of BPA occurs only during the initial addition of BPA into the reactor (i.e., 14.3 ± 7.4% sorbed; Table S2). The low steady-state concentration of sorbed BPA supports the supposition that the formation of the surface complex is the rate-limiting step in BPA degradation rather than the first electron transfer,[2,6,7,40] and suggests that the starting material has a higher binding affinity to BPA than the reacted material. Sorption of produced HCA is very small over all three additions (i.e., < 1.0 ± 0.9%). This relative trend between BPA and HCA sorption is in agreement with the reported octanol−water partitioning coefficient (K_{ow}) of HCA being much smaller than that of BPA (log K_{ow} of 0.76 and 2.76, respectively),[30] and the reported solubility of HCA being much higher than BPA (2.65 and 0.31 g/L, respectively).[30]

The oxidation of BPA produces a suite of organic products,[15] which may have different affinity for the mineral surface. For example, polymeric products produced by radical coupling are more likely to sorb to the mineral surface due to their larger size and decreased polarity and may prevent sorption of BPA during sequential exposures. However, no major product peaks with longer retention times than BPA, indicative of polymeric products, are observed by HPLC with either UV or fluorescence detection (Figures S9 and S10), while many peaks with shorter retention times are present in the chromatograms. Although identification of additional BPA oxidation products is beyond the scope of this study, the HPLC results indicate that many of the oxidation products are highly polar and that minimal polymeric products are produced in this reaction. While sorption of HCA does not appear to play a role in obscuring reaction sites because it sorbs less strongly than BPA, the relative sorption of other proposed organic products[15] warrants further investigation. Collectively, the relative sorption of BPA and HCA (Table S2), the absence of less-polar products (Figures S9 and S10), and the decreased sorption of phenols at circumneutral pH values[26] suggest that sorption of organics does not contribute to the decrease in BPA oxidation rate observed over 12 sequential additions.

Solid-Phase Accumulation of Reduced Manganese. The production of reduced manganese could decrease the organic compound reaction rate by obscuring reactive sites on the mineral surface or by competitively reacting with the mineral surface. This mechanism has been proposed as an explanation for the deviation from pseudo-first-order kinetics during the oxidation of several classes of antibacterial agents,[26,40,72] halogenated phenols,[68,74] and naproxen[75] by MnO_2. Furthermore, the addition of aqueous Mn(II) consistently results in inhibition of BPA oxidation by Mn oxides.[14,15,45]

Corner-sharing Mn is detected after the fourth addition of BPA, and its coordination number increases throughout 12 additions of the target compound (Figure 3b). Corner-sharing Mn is assumed to be Mn(III) or Mn(II) in interlayer positions. Surface-bound Mn(II) also increases after the fourth addition of BPA, as measured by Ca^{2+} exchange (Figure S16). In contrast, aqueous Mn(II) is not detected until after six additions of BPA (Figure 1c). Stone and Ulrich demonstrate that the desorption of Mn(II) from the surface of the mineral is a slow reaction compared to the desorption of organic molecules.[76] This observation is confirmed in this study as Mn(II) is detected on the solid before it appears in solution (i.e., addition 4 compared to addition 6; Figures S16 and 1c). Our results show that accumulation of aqueous Mn(II) over sequential additions of BPA corresponds with the decrease in BPA oxidation rate (Figure 1). Therefore, the production of Mn(II), which may arise from Mn(III) reduction or disproportionation, is a likely cause of decreasing MnO_2 reactivity with BPA. Additionally, while bulk measurements of the oxidation state remain relatively constant throughout 12 additions of BPA, XPS reveals that Mn(III) preferentially accumulates at the mineral surface (Figure 3a). The increase of Mn(III) at the mineral surface likely contributes to the decreased transformation rate of BPA, even in the absence of large changes in the bulk MnO_2 oxidation state. It is unlikely that the increase in Mn(III) is due to comproportionation of Mn(II) and Mn(IV), which would lead to the formation of orthogonal layered birnessite detectable by changes in the XRD pattern.[77]

Structural Changes. Changes to the mineral structure consist predominantly of the increase in interlayer Mn. Interlayer Mn could be Mn(II) or Mn(III) and exhibits corner-sharing geometry, as shown in the EXAFS model (Figure 3b). The increase of interlayer Mn is corroborated by the analysis of the diffraction patterns (Figure S15), which show a decrease in the high-angle scattering tail of the peak at 37° and the appearance of a characteristic dip at 47°, both of which indicate capping of vacancies by metal cations (i.e., Mn(II) or Mn(III)).[33,47,48,78,79] Previous studies have reported

DOI: 10.1021/acs.est.6b05904
Environ. Sci. Technol. XXXX, XXX, XXX−XXX

that these cation vacancy sites are of critical importance in adsorption and electron transfer processes that occur on the mineral surface.[50,80,81]

Changes in HCA Yield. Another example of the importance of quantifying changes in both aqueous- and solid-phase geochemistry is the 10-fold decrease in HCA yield over 12 sequential additions of BPA (Figure 1b). The initial yield of HCA from BPA oxidation ranges from 32−39.7% in this study. In comparison, earlier work reports yields up to 64% under similar conditions (e.g., pH 7.4); however, the MnO_2 used in the previous study is synthesized under hydrothermal conditions[30] and is likely more crystalline than the solid used in the present study. During the 12th addition of BPA, only 3.5% of oxidized BPA is converted to HCA. Therefore, the production or relative stability of other transformation products becomes more important as the MnO_2 solids undergo repeated reaction with BPA. Previous studies have identified 11 of the numerous products that form through radical coupling, fragmentation, substitution, and elimination, including HCA.[15,30] Regardless of the identity of the suite of oxidation products, the mechanism of BPA oxidation and importance of HCA as a major product clearly changes as repeated additions to MnO_x alter the reactivity of the Mn oxide. These results suggest that the products or yields identified in single-addition batch reactors may not be representative for more complex environments.

Conceptual Framework. By systematically quantifying changes in the mineral structure during BPA oxidation by MnO_x, it is possible to develop a conceptual model that provides direct evidence to explain why the reactivity of the mineral toward BPA decreases with time. The Mn(III)-rich δ-MnO_2 starting material contains no detectable interlayer Mn, indicating the Mn(III) is located within the octahedral sheets. After diffusion of the phenol to the mineral surface and formation of a surface complex, the organic compound is oxidized through a one-electron transfer and Mn(IV) is reduced to Mn(III).[6,25,27,28] The Mn(III) may then either remain in the interlayer, disproportionate to Mn(II) and Mn(IV), undergo a second one-electron transfer with BPA or its degradation products to produce Mn(II), or migrate to a vacancy site in the octahedral sheet. Mn(III) does not appear to play a primary role in the transformation of BPA because BPA oxidation rates decline despite Mn(III) accumulation during the first five BPA additions. The data also suggest that, at a predominance above 40%, surficial Mn(III) is consumed by disproportionation to Mn(II) and Mn(IV), resulting in the decrease in surface Mn(III) and production of Mn(IV) and Mn(II) at the surface. Mn(III) does not appear to fill in vacancy sites as the fractional occupancy of the material does not notably increase over BPA additions (Figure 3b). Mn(II) accumulates on the mineral surface (Figure S16) until it reaches saturation.[6,7,39] After this point, excess Mn(II) dissolves and is detected in solution (Figure 1c). As a result, the overall oxidation state of the Mn oxide remains within 3.60 ± 0.07 valence units (Figure S13) despite extensive reaction with BPA. With increasing BPA additions, reduced Mn centers migrate to the interlayer, capping highly reactive vacancy sites (Figures 3b and S15). By the use of BPA oxidation kinetics as a way to probe the reactivity of MnO_2 (Figure 1a), it is clear that changes in reactivity due to accumulation of interlayer Mn and Mn(II) on the surface of the mineral happen prior to the appearance of dissolved Mn(II), emphasizing the importance of these structural changes to the mineral. The accumulation of reduced manganese within the mineral, and ultimately in solution, is also correlated with the change in HCA yield (Figure 1b), suggesting that mineral transformation alters the mechanism of BPA oxidation and its intermediate products. In contrast, the observed decrease in BPA oxidation rate is not associated with changes in surface area, sorption of organics, or a change in bulk MnO_x oxidation state.

Environmental Implications. BPA is an endocrine-disrupting compound[18] that is found in elevated concentrations in many aquatic environments.[23,82] It is especially damaging to fish and other aquatic species.[19] Manganese oxides are found in high concentrations in the environment as well, primarily in soils and sediments.[83] Oxidation by MnO_2 is a potential fate for BPA in the environment. The formation of HCA as an oxidation product of BPA could have effects on the environment because HCA is more mobile[30] and less susceptible to oxidation by MnO_2. It may also be more estrogenic than BPA; an in vitro estrogen receptor binding assay suggests that HCA has 100-fold higher binding affinity to the estrogen receptor than BPA.[51] Nevertheless, HCA is removed by Mn oxides, albeit at a slower rate.

The transformation of phenolic contaminants by Mn(III/IV) oxides could potentially be used in wastewater, urban stormwater, or landfill leachate treatment,[84] preventing BPA, HCA, and other phenolic compounds from entering natural waters and disrupting wildlife ecosystems. Manganese oxides are capable of transforming a range of organic compounds, including antibacterial agents,[26,40,42,46,69,72,85−91] polyaminocarboxylate ligands,[92] endocrine disruptors,[43,44,46,93−95] brominated flame retardants,[96] rubber additives,[97] pain relievers,[75,98] and antiepileptic pharmaceuticals.[73] The comprehensive approach used here provides details required for the implementation of Mn oxides for water treatment, such as the mechanism, mineralogical changes, and changes in kinetics.

■ ASSOCIATED CONTENT

Supporting Information

The Supporting Information is available free of charge on the ACS Publications website at DOI: 10.1021/acs.est.6b05904.

Additional details on materials, analytical methods, rate constant analysis, HCA detection and yield calculation, sorption analysis, and solids analysis. Figures showing synthesis reactions, mass spectra, HPLC chromatographs, rate analysis, UV spectra, a batch reaction, XPS data, fitted XANES data, oxidation state, raw and modeled data of the chi functions and relative radial distribution function, crystallinity, and surface-bound Mn. A table showing the percentage of BPA recovered, percentages of BPA and HCA, BET analysis, and EXAFS fitting results. (PDF)

■ AUTHOR INFORMATION

Corresponding Authors

*Phone: (608) 262-1820; fax: (608) 262-0454; e-mail: remucal@wisc.edu.

*Phone: (608) 262-0768; fax: (608) 262-0454; e-mail: mgindervogel@wisc.edu.

ORCID

Christina K. Remucal: 0000-0003-4285-7638

Matthew Ginder-Vogel: 0000-0001-9183-1931

Notes

The authors declare no competing financial interest.

DOI: 10.1021/acs.est.6b05904
Environ. Sci. Technol. XXXX, XXX, XXX−XXX

■ ACKNOWLEDGMENTS

The authors thank Eugene Ilton at the Pacific Northwest National Laboratory for his advice and help in fitting XPS data. This work was performed at GeoSoilEnviroCARS (The University of Chicago, Sector 13) Advanced Photon Source, Argonne National Laboratory. GeoSoilEnviroCARS is supported by the National Science Foundation (NSF; EAR-1128799) and the Department of Energy (DE-FG02-94ER14466). This research used resources of the Advanced Photon Source, a U.S. Department of Energy (DOE) Office of Science User Facility operated for the DOE Office of Science by Argonne National Laboratory under contract no. DE-AC02-06CH11357. Funding for this study was provided by NSF (CBET 1509879) and the Wisconsin Groundwater Coordinating Council. This material is based upon work supported by the National Science Foundation Graduate Research Fellowship Program under grant no. DGE-1256259. Any opinions, findings, and conclusions or recommendations expressed in this material are those of the authors and do not necessarily reflect the views of the National Science Foundation.

■ REFERENCES

(1) Eary, L. E.; Rai, D. Kinetics of chromium(III) oxidation to chromium(VI) by reaction with manganese dioxide. *Environ. Sci. Technol.* **1987**, *21* (12), 1187−1193.
(2) Lafferty, B. J.; Ginder-Vogel, M.; Sparks, D. L. Arsenite oxidation by a poorly-crystalline manganese oxide. 3. Arsenic and manganese desorption. *Environ. Sci. Technol.* **2011**, *45* (21), 9218−9223.
(3) Landrot, G.; Ginder-Vogel, M.; Livi, K.; Fitts, J. P.; Sparks, D. L. Chromium(III) oxidation by three poorly crystalline manganese(IV) oxides. 2. Solid phase analyses. *Environ. Sci. Technol.* **2012**, *46* (21), 11601−11609.
(4) Tournassat, C.; Charlet, L.; Bosbach, D.; Manceau, A. Arsenic(III) oxidation by birnessite and precipitation of manganese(II) arsenate. *Environ. Sci. Technol.* **2002**, *36* (3), 493−500.
(5) Remucal, C. K.; Ginder-Vogel, M. A critical review of the reactivity of manganese oxides with organic contaminants. *Environ. Sci. Process. Impacts* **2014**, *16* (6), 1247−1266.
(6) Stone, A. T. Reductive dissolution of manganese(III/IV) oxides by substituted phenols. *Environ. Sci. Technol.* **1987**, *21* (10), 979−988.
(7) Stone, A. T.; Morgan, J. J. Reduction and dissolution of manganese(III) and manganese(IV) oxides by organics. 1. Reaction with hydroquinone. *Environ. Sci. Technol.* **1984**, *18* (6), 450−456.
(8) Xyla, A. G.; Sulzberger, B.; Luther, G. W., III; Hering, J. G.; Van Cappellen, P.; Stumm, W. Reductive dissolution of manganese(III,IV) (hydr)oxides by oxalate: The effect of pH and light. *Langmuir* **1992**, *8* (1), 95−103.
(9) Dick, G. J.; Lee, Y. E.; Tebo, B. M. Manganese(II)-oxidizing *Bacillus* spores in Guaymas Basin hydrothermal sediments and plumes. *Appl. Environ. Microbiol.* **2006**, *72* (5), 3184−3190.
(10) Negra, C.; Ross, D. S.; Lanzirotti, A. Oxidizing behavior of soil manganese. *Soil Sci. Soc. Am. J.* **2005**, *69* (1), 87−95.
(11) Post, J. E. Manganese oxide minerals: Crystal structures and economic and environmental significance. *Proc. Natl. Acad. Sci. U. S. A.* **1999**, *96* (7), 3447−3454.
(12) Tani, Y.; Miyata, N.; Iwahori, K.; Soma, M.; Tokuda, S.; Seyama, H.; Theng, B. K. Biogeochemistry of manganese oxide coatings on pebble surfaces in the Kikukawa River System, Shizuoka, Japan. *Appl. Geochem.* **2003**, *18* (10), 1541−1554.
(13) Wehrli, B.; Friedl, G.; Manceau, A. Reaction rates and products of manganese oxidation at the sediment-water interface. In *Aquatic Chemistry*; American Chemical Society: Washington, DC, 1995; Vol. *244*, pp 111−134.
(14) Gao, N.; Hong, J.; Yu, Z.; Peng, P.; Huang, W. Transformation of bisphenol A in the presence of manganese dioxide. *Soil Sci.* **2011**, *176* (6), 265−272.
(15) Lin, K.; Liu, W.; Gan, J. Oxidative removal of bisphenol A by manganese dioxide: Efficacy, products, and pathways. *Environ. Sci. Technol.* **2009**, *43* (10), 3860−3864.
(16) Lin, K.; Peng, Y.; Huang, X.; Ding, J. Transformation of bisphenol A by manganese oxide-coated sand. *Environ. Sci. Pollut. Res.* **2013**, *20* (3), 1461−1467.
(17) Bisphenol A (BPA) Information & Resources. http://www.bisphenol-a.org/ (accessed Sep 6, 2016).
(18) Vandenberg, L. N.; Hauser, R.; Marcus, M.; Olea, N.; Welshons, W. V. Human exposure to bisphenol A (BPA). *Reprod. Toxicol.* **2007**, *24* (2), 139−177.
(19) Canesi, L.; Fabbri, E. Environmental effects of BPA: Focus on aquatic species. *Dose-Response* **2015**, *13* (3), 1−14.
(20) Tan, B. L. L.; Hawker, D. W.; Müller, J. F.; Leusch, F. D. L.; Tremblay, L. A.; Chapman, H. F. Modelling of the fate of selected endocrine disruptors in a municipal wastewater treatment plant in South East Queensland, Australia. *Chemosphere* **2007**, *69* (4), 644−654.
(21) Masoner, J. R.; Kolpin, D. W.; Furlong, E. T.; Cozzarelli, I. M.; Gray, J. L.; Schwab, E. A. Contaminants of emerging concern in fresh leachate from landfills in the conterminous United States. *Env. Sci. Process. Impacts* **2014**, *16* (10), 2335−2354.
(22) Yu, X.; Xue, J.; Yao, H.; Wu, Q.; Venkatesan, A. K.; Halden, R. U.; Kannan, K. Occurrence and estrogenic potency of eight bisphenol analogs in sewage sludge from the U.S. EPA targeted national sewage sludge survey. *J. Hazard. Mater.* **2015**, *299*, 733−739.
(23) Baldwin, A. K.; Corsi, S. R.; De Cicco, L. A.; Lenaker, P. L.; Lutz, M. A.; Sullivan, D. J.; Richards, K. D. Organic contaminants in Great Lakes tributaries: Prevalence and potential aquatic toxicity. *Sci. Total Environ.* **2016**, *554*−*555*, 42−52.
(24) Belfroid, A.; van Velzen, M.; van der Horst, B.; Vethaak, D. Occurrence of bisphenol A in surface water and uptake in fish: Evaluation of field measurements. *Chemosphere* **2002**, *49* (1), 97−103.
(25) Laha, S.; Luthy, R. G. Oxidation of aniline and other primary aromatic amines by manganese dioxide. *Environ. Sci. Technol.* **1990**, *24* (3), 363−373.
(26) Zhang, H.; Huang, C.-H. Oxidative transformation of triclosan and chlorophene by manganese oxides. *Environ. Sci. Technol.* **2003**, *37* (11), 2421−2430.
(27) Jiang, J.; Gao, Y.; Pang, S.-Y.; Lu, X.-T.; Zhou, Y.; Ma, J.; Wang, Q. Understanding the role of manganese dioxide in the oxidation of phenolic compounds by aqueous permanganate. *Environ. Sci. Technol.* **2015**, *49* (1), 520−528.
(28) Ukrainczyk, L.; McBride, M. B. Oxidation of phenol in acidic aqueous suspensions of manganese oxides. *Clays Clay Miner.* **1992**, *40* (2), 157−166.
(29) Stone, A. T.; Morgan, J. J. Reduction and dissolution of manganese(III) and manganese(IV) oxides by organics: 2. Survey of the reactivity of organics. *Environ. Sci. Technol.* **1984**, *18* (8), 617−624.
(30) Im, J.; Prevatte, C. W.; Campagna, S. R.; Löffler, F. E. Identification of 4-hydroxycumyl alcohol as the major MnO_2-mediated bisphenol A transformation product and evaluation of its environmental fate. *Environ. Sci. Technol.* **2015**, *49* (10), 6214−6221.
(31) Nico, P. S.; Zasoski, R. J. Mn(III) center availability as a rate controlling factor in the oxidation of phenol and sulfide on δ-MnO_2. *Environ. Sci. Technol.* **2001**, *35* (16), 3338−3343.
(32) Cui, H.; Liu, X.; Tan, W.; Feng, X.; Liu, F.; Daniel Ruan, H. Influence of Mn(III) availability on the phase transformation from layered buserite to tunnel-structured todorokite. *Clays Clay Miner.* **2008**, *56* (4), 397−403.
(33) Drits, V. A.; Lanson, B.; Gaillot, A.-C. Birnessite polytype systematics and identification by powder X-ray diffraction. *Am. Mineral.* **2007**, *92* (5−6), 771−788.
(34) Kwon, K. D.; Refson, K.; Sposito, G. Defect-induced photoconductivity in layered manganese oxides: A density functional theory study. *Phys. Rev. Lett.* **2008**, *100* (14), 146601.
(35) Lanson, B.; Drits, V. A.; Gaillot, A.-C.; Silvester, E.; Plançon, A.; Manceau, A. Structure of heavy-metal sorbed birnessite: Part 1. Results from X-ray diffraction. *Am. Mineral.* **2002**, *87* (11−12), 1631−1645.

DOI: 10.1021/acs.est.6b05904
Environ. Sci. Technol. XXXX, XXX, XXX−XXX

(36) Manceau, A.; Drits, V. A.; Silvester, E.; Bartoli, C.; Lanson, B. Structural mechanism of Co^{2+} oxidation by the phyllomanganate buserite. *Am. Mineral.* **1997**, *82* (11−12), 1150−1175.
(37) Zhao, W.; Cui, H.; Liu, F.; Tan, W.; Feng, X. Relationship between Pb^{2+} adsorption and average Mn oxidation state in synthetic birnessites. *Clays Clay Miner.* **2009**, *57* (5), 513−520.
(38) Zhu, M.; Ginder-Vogel, M.; Parikh, S. J.; Feng, X.-H.; Sparks, D. L. Cation effects on the layer structure of biogenic Mn-oxides. *Environ. Sci. Technol.* **2010**, *44* (12), 4465−4471.
(39) McBride, M. B. Adsorption and oxidation of phenolic compounds by iron and manganese oxides. *Environ. Toxicol. Chem.* **1987**, *51* (6), 1466−1472.
(40) Zhang, H.; Chen, W.-R.; Huang, C.-H. Kinetic modeling of oxidation of antibacterial agents by manganese oxide. *Environ. Sci. Technol.* **2008**, *42* (15), 5548−5554.
(41) Klausen, J.; Haderlein, S. B.; Schwarzenbach, R. P. Oxidation of substituted anilines by aqueous MnO_2: Effect of co-solutes on initial and quasi-steady-state kinetics. *Environ. Sci. Technol.* **1997**, *31* (9), 2642−2649.
(42) Rubert, K. F.; Pedersen, J. A. Kinetics of oxytetracycline reaction with a hydrous manganese oxide. *Environ. Sci. Technol.* **2006**, *40* (23), 7216−7221.
(43) Xu, L.; Xu, C.; Zhao, M.; Qiu, Y.; Sheng, G. Oxidative removal of aqueous steroid estrogens by manganese oxides. *Water Res.* **2008**, *42* (20), 5038−5044.
(44) Lu, Z.; Lin, K.; Gan, J. Oxidation of bisphenol F (BPF) by manganese dioxide. *Environ. Pollut.* **2011**, *159* (10), 2546−2551.
(45) Zhang, T.; Zhang, X.; Yan, X.; Ng, J.; Wang, Y.; Sun, D. D. Removal of bisphenol A via a hybrid process combining oxidation on β-MnO_2 nanowires with microfiltration. *Colloids Surf., A* **2011**, *392* (1), 198−204.
(46) Shaikh, N.; Taujale, S.; Zhang, H.; Artyushkova, K.; Ali, A.-M. S.; Cerrato, J. M. Spectroscopic investigation of interfacial interaction of manganese oxide with triclosan, aniline, and phenol. *Environ. Sci. Technol.* **2016**, *50* (20), 10978−10987.
(47) Drits, V. A.; Silvester, E.; Gorshkov, A. I.; Manceau, A. Structure of synthetic monoclinic Na-rich birnessite and hexagonal birnessite: I. Results from X-ray diffraction and selected-area electron diffraction. *Am. Mineral.* **1997**, *82* (9), 946−961.
(48) Silvester, E.; Manceau, M.; Drits, V. A. Structure of synthetic monoclinic Na-rich birnessite and hexagonal birnessite: II. Results from chemical studies and EXAFS spectroscopy. *Am. Mineral.* **1997**, *82*, 962−978.
(49) Tan, W.; Lu, S.; Liu, F.; Feng, X.; He, J.; Koopal, L. K. Determination of the point-of-zero charge of manganese oxides with different methods including an improved salt titration method. *Soil Sci.* **2008**, *173* (4), 277−286.
(50) Lafferty, B. J.; Ginder-Vogel, M.; Zhu, M.; Livi, K. J. T.; Sparks, D. L. Arsenite oxidation by a poorly crystalline manganese-oxide. 2. Results from X-ray absorption spectroscopy and X-ray diffraction. *Environ. Sci. Technol.* **2010**, *44* (22), 8467−8472.
(51) Nakamura, S.; Tezuka, Y.; Ushiyama, A.; Kawashima, C.; Kitagawara, Y.; Takahashi, K.; Ohta, S.; Mashino, T. Ipso substitution of bisphenol A catalyzed by microsomal cytochrome P450 and enhancement of estrogenic activity. *Toxicol. Lett.* **2011**, *203* (1), 92−95.
(52) Piper, D. Z.; Basler, J. R.; Bischoff, J. L. Oxidation state of marine manganese nodules. *Geochim. Cosmochim. Acta* **1984**, *48* (11), 2347−2355.
(53) Murray, J. W.; Balistrieri, L. S.; Paul, B. The oxidation state of manganese in marine sediments and ferromanganese nodules. *Geochim. Cosmochim. Acta* **1984**, *48* (6), 1237−1247.
(54) Freeman, D. S.; Chapman, W. G. An improved oxalate method for the determination of active oxygen in manganese dioxide. *Analyst* **1971**, *96* (1149), 865−869.
(55) Good, N. E.; Winget, G. D.; Winter, W.; Connolly, T. N.; Izawa, S.; Singh, R. M. Hydrogen ion buffers for biological research. *Biochemistry* **1966**, *5* (2), 467−477.
(56) Ferreira, C. M. H.; Pinto, I. S. S.; Soares, E. V.; Soares, H. M. V. M. (Un)suitability of the use of pH buffers in biological, biochemical and environmental studies and their interaction with metal ions − a review. *RSC Adv.* **2015**, *5* (39), 30989−31003.
(57) Ying, S. C.; Kocar, B. D.; Fendorf, S. Oxidation and competitive retention of arsenic between iron- and manganese oxides. *Geochim. Cosmochim. Acta* **2012**, *96*, 294−303.
(58) Ilton, E. S.; Post, J. E.; Heaney, P. J.; Ling, F. T.; Kerisit, S. N. XPS determination of Mn oxidation states in Mn (hydr)oxides. *Appl. Surf. Sci.* **2016**, *366*, 475−485.
(59) Webb, S. M. SIXpack: A graphical user interface for XAS analysis using IFEFFIT. *Phys. Scr.* **2005**, *2005* (T115), 1011−1014.
(60) Manceau, A.; Marcus, M. A.; Grangeon, S. Determination of Mn valence states in mixed-valent manganates by XANES spectroscopy. *Am. Mineral.* **2012**, *97* (5−6), 816−827.
(61) Webb, S. M. Structural characterization of biogenic Mn oxides produced in seawater by the marine *Bacillus* sp. strain SG-1. *Am. Mineral.* **2005**, *90* (8−9), 1342−1357.
(62) Rehr, J. J.; Albers, R. C.; Zabinsky, S. I. High-order multiple-scattering calculations of X-ray-absorption fine structure. *Phys. Rev. Lett.* **1992**, *69* (23), 3397−3400.
(63) Newville, M. IFEFFIT: Interactive XAFS analysis and FEFF fitting. *J. Synchrotron Radiat.* **2001**, *8* (2), 322−324.
(64) Lanson, B.; Drits, V. A.; Silvester, E.; Manceau, A. Structure of H-exchanged hexagonal birnessite and its mechanism of formation from Na-rich monoclinic buserite at low pH. *Am. Mineral.* **2000**, *85* (5−6), 826−838.
(65) Klewicki, J. K.; Morgan, J. J. Kinetic behavior of Mn(III) complexes of pyrophosphate, EDTA, and citrate. *Environ. Sci. Technol.* **1998**, *32* (19), 2916−2922.
(66) Pizzigallo, M. D.; Ruggiero, P.; Crecchio, C.; Mascolo, G. Oxidation of chloroanilines at metal oxide surfaces. *J. Agric. Food Chem.* **1998**, *46* (5), 2049−2054.
(67) Ulrich, H. J.; Stone, A. T. The oxidation of chlorophenols adsorbed to manganese oxide surfaces. *Environ. Sci. Technol.* **1989**, *23* (4), 421−428.
(68) Lin, K.; Yan, C.; Gan, J. Production of hydroxylated polybrominated diphenyl ethers (OH-PBDEs) from bromophenols by manganese dioxide. *Environ. Sci. Technol.* **2014**, *48* (1), 263−271.
(69) Xiao, X.; Sun, S.-P.; McBride, M. B.; Lemley, A. T. Degradation of ciprofloxacin by cryptomelane-type manganese(III/IV) oxides. *Environ. Sci. Pollut. Res.* **2013**, *20* (1), 10−21.
(70) Liu, C. S.; Zhang, L. J.; Feng, C. H.; Wu, C. A.; Li, F. B.; Li, X. Z. Relationship between oxidative degradation of 2-mercaptobenzothiazole and physicochemical properties of manganese (hydro)oxides. *Environ. Chem.* **2009**, *6* (1), 83.
(71) Bialk, H. M.; Simpson, A. J.; Pedersen, J. A. Cross-coupling of sulfonamide antimicrobial agents with model humic constituents. *Environ. Sci. Technol.* **2005**, *39* (12), 4463−4473.
(72) Chen, W.-R.; Ding, Y.; Johnston, C. T.; Teppen, B. J.; Boyd, S. A.; Li, H. Reaction of lincosamide antibiotics with manganese oxide in aqueous solution. *Environ. Sci. Technol.* **2010**, *44* (12), 4486−4492.
(73) He, Y.; Xu, J.; Zhang, Y.; Guo, C.; Li, L.; Wang, Y. Oxidative transformation of carbamazepine by manganese oxides. *Environ. Sci. Pollut. Res.* **2012**, *19* (9), 4206−4213.
(74) Petrie, R. A.; Grossl, P. R.; Sims, R. C. Oxidation of pentachlorophenol in manganese oxide suspensions under controlled E_h and pH environments. *Environ. Sci. Technol.* **2002**, *36* (17), 3744−3748.
(75) Zhang, Y.; Yang, Y.; Zhang, Y.; Zhang, T.; Ye, M. Heterogeneous oxidation of naproxen in the presence of α-MnO_2 nanostructures with different morphologies. *Appl. Catal., B* **2012**, *127*, 182−189.
(76) Stone, A. T.; Ulrich, H. J. Kinetics and reaction stoichiometry in reductive dissolution of manganese(IV) dioxide and Co(III) oxide by hydroquinone. *J. Colloid Interface Sci.* **1989**, *132* (2), 509−522.
(77) Feng, X. H.; Zhu, M.; Ginder-Vogel, M.; Ni, C.; Parikh, S. J.; Sparks, D. L. Formation of nano-crystalline todorokite from biogenic Mn oxides. *Geochim. Cosmochim. Acta* **2010**, *74* (11), 3232−3245.

DOI: 10.1021/acs.est.6b05904
Environ. Sci. Technol. XXXX, XXX, XXX−XXX

(78) Villalobos, M.; Toner, B.; Bargar, J.; Sposito, G. Characterization of the manganese oxide produced by *Pseudomonas putida* strain MnB1. *Geochim. Cosmochim. Acta* **2003**, *67* (14), 2649−2662.
(79) Villalobos, M.; Lanson, B.; Manceau, A.; Toner, B.; Sposito, G. Structural model for the biogenic Mn oxide produced by *Pseudomonas putida*. *Am. Mineral.* **2006**, *91* (4), 489−502.
(80) Grangeon, S.; Manceau, A.; Guilhermet, J.; Gaillot, A.-C.; Lanson, M.; Lanson, B. Zn sorption modifies dynamically the layer and interlayer structure of vernadite. *Geochim. Cosmochim. Acta* **2012**, *85*, 302−313.
(81) Grangeon, S.; Lanson, B.; Lanson, M.; Manceau, A. Crystal structure of Ni-sorbed synthetic vernadite: A powder X-ray diffraction study. *Mineral. Mag.* **2008**, *72* (6), 1279−1291.
(82) Kolpin, D. W.; Furlong, E. T.; Meyer, M. T.; Thurman, E. M.; Zaugg, S. D.; Barber, L. B.; Buxton, H. T. Pharmaceuticals, hormones, and other organic wastewater contaminants in U.S. streams, 1999−2000: A national reconnaissance. *Environ. Sci. Technol.* **2002**, *36* (6), 1202−1211.
(83) Smith, R. A.; Alexander, R. B.; Wolman, G. M. Water-quality trends in the nation's rivers. *Science* **1987**, *235* (4796), 1607−1615.
(84) Grebel, J. E.; Charbonnet, J. A.; Sedlak, D. L. Oxidation of organic contaminants by manganese oxide geomedia for passive urban stormwater treatment systems. *Water Res.* **2016**, *88*, 481−491.
(85) Chen, W.-R.; Huang, C.-H. Transformation of tetracyclines mediated by Mn(II) and Cu(II) ions in the presence of oxygen. *Environ. Sci. Technol.* **2009**, *43* (2), 401−407.
(86) Dong, J.; Li, Y.; Zhang, L.; Liu, C.; Zhuang, L.; Sun, L.; Zhou, J. The oxidative degradation of sulfadiazine at the interface of α-MnO_2 and water: Degradation of antibiotics by manganese dioxides. *J. Chem. Technol. Biotechnol.* **2009**, *84* (12), 1848−1853.
(87) Feitosa-Felizzola, J.; Hanna, K.; Chiron, S. Adsorption and transformation of selected human-used macrolide antibacterial agents with iron(III) and manganese(IV) oxides. *Environ. Pollut.* **2009**, *157* (4), 1317−1322.
(88) Liu, C.; Zhang, L.; Li, F.; Wang, Y.; Gao, Y.; Li, X.; Cao, W.; Feng, C.; Dong, J.; Sun, L. Dependence of sulfadiazine oxidative degradation on physicochemical properties of manganese dioxides. *Ind. Eng. Chem. Res.* **2009**, *48* (23), 10408−10413.
(89) Chen, W.-R.; Huang, C.-H. Transformation kinetics and pathways of tetracycline antibiotics with manganese oxide. *Environ. Pollut.* **2011**, *159* (5), 1092−1100.
(90) Chen, G.; Zhao, L.; Dong, Y. Oxidative degradation kinetics and products of chlortetracycline by manganese dioxide. *J. Hazard. Mater.* **2011**, *193*, 128−138.
(91) Gao, J.; Hedman, C.; Liu, C.; Guo, T.; Pedersen, J. A. Transformation of sulfamethazine by manganese oxide in aqueous solution. *Environ. Sci. Technol.* **2012**, *46* (5), 2642−2651.
(92) McArdell, C. S.; Stone, A. T.; Tian, J. Reaction of EDTA and related aminocarboxylate chelating agents with $Co^{III}OOH$ (heterogenite) and $Mn^{III}OOH$ (manganite). *Environ. Sci. Technol.* **1998**, *32* (19), 2923−2930.
(93) Jiang, L.; Huang, C.; Chen, J.; Chen, X. Oxidative transformation of 17β-estradiol by MnO_2 in aqueous solution. *Arch. Environ. Contam. Toxicol.* **2009**, *57* (2), 221−229.
(94) Rudder, J. d.; Wiele, T. V.; Dhooge, W.; Comhaire, F.; Verstraete, W. Advanced water treatment with manganese oxide for the removal of 17α-ethynylestradiol (EE2). *Water Res.* **2004**, *38* (1), 184−192.
(95) Kim, D.-G.; Jiang, S.; Jeong, K.; Ko, S.-O. Removal of 17α-ethinylestradiol by biogenic manganese oxides produced by the *Pseudomonas putida* strain MnB1. *Water, Air, Soil Pollut.* **2012**, *223* (2), 837−846.
(96) Lin, K.; Liu, W.; Gan, J. Reaction of tetrabromobisphenol A (TBBPA) with manganese dioxide: Kinetics, products, and pathways. *Environ. Sci. Technol.* **2009**, *43* (12), 4480−4486.
(97) Dong, J.; Zhang, L.; Liu, H.; Liu, C.; Gao, Y.; Sun, L. The oxidative degradation of 2-mercaptobenzothialzole by different manganese dioxides. *Fresenius Environ. Bull.* **2010**, *19*, 1615−1622.
(98) Xiao, H.; Song, H.; Xie, H.; Huang, W.; Tan, J.; Wu, J. Transformation of acetaminophen using manganese dioxide − mediated oxidative processes: Reaction rates and pathways. *J. Hazard. Mater.* **2013**, *250*−*251*, 138−146.

DOI: 10.1021/acs.est.6b05904
Environ. Sci. Technol. XXXX, XXX, XXX−XXX